An AIE Metal Iridium Complex: Photophysical Properties and Singlet Oxygen Generation Capacity

Weijin Zhu , Shengnan Liu , Ziwei Wang , Chunguang Shi , Qiaohua Zhang , Zihan Wu , Guangzhe Li * , Dongxia Zhu *

Posted Date: 7 November 2023

doi: 10.20944/preprints202311.0430.v1

Keywords: aggregation-induced emission (AIE); Iridium(III) complex; phosphorescence; singlet oxygen (1O2)

Article

An AIE Metal Iridium Complex: Photophysical Properties and Singlet Oxygen Generation Capacity

Weijin Zhu [1], Shengnan Liu [1], Ziwei Wang [1], Chunguang Shi [1], Qiaohua Zhang [1], Zihan Wu [1], Guangzhe Li [2,*] and Dongxia Zhu [1,*]

[1] Key Laboratory of Nanobiosensing and Nanobioanalysis at Universities of Jilin Province, Department of Chemistry, Northeast Normal University, 5268 Renmin Street, Changchun 130117, China; zhudx047@nenu.edu.cn
[2] Jilin Provincial Science and Technology Innovation Center of Health Food of Chinese Medicine, Changchun University of Chinese Medicine, Changchun 130117, China; 1993008106@qq.com
* Correspondence: zhudx047@nenu.edu.cn (D.Z.); 1993008106@qq.com (G.L.)

Abstract: Photodynamic therapy (PDT) has garnered significant attention in the fields of cancer treatment and drug-resistant bacteria eradication due to its non-invasive nature and spatiotemporal controllability. Iridium complexes have captivated researchers owing to their tunable structure, exceptional optical properties, and substantial Stokes displacement. However, most of these complexes suffer from aggregation-induced quenching, leading to diminished luminous efficiency. In contrast to conventional photosensitizers, photosensitizers exhibiting aggregation-induced luminescence (AIE) properties retain the ability to generate a large number of reactive oxygen species when aggregated. To overcome these limitations, we designed and synthesized a novel iridium complex named **Ir-TPA** in this study. It incorporates quinoline triphenylamine cyclomethylated ligands that confer AIE characteristics for **Ir-TPA**. We systematically investigated the photophysical properties, AIE behavior, spectral features, and reactive oxygen generation capacity of **Ir-TPA**. The results demonstrate that **Ir-TPA** exhibits excellent optical properties with pronounced AIE phenomenon and robust capability for producing singlet oxygen species. This work not only introduces a new class of metal iridium complex photosensitizer with AIE attributes but also holds promise for achieving remarkable photodynamic therapeutic effects in future cellular experiments and biological studies.

Keywords: aggregation-induced Emission (AIE); iridium(III) complex; phosphorescence; singlet oxygen ($^1O_2$)

1. Introduction

Photodynamic therapy is a selective process in which photosensitizer molecules absorb the appropriate wavelength of light and initiate the photoactivation process to produce toxic substances, thus leading to apoptosis or necrosis of pathological tissue cells[1,2]. Photodynamic therapy (PDT) has attracted extensive attention from researchers due to its advantages such as non-invasive, spatiotemporal controllability, and not easy to induce drug resistance [3-5]. In the PDT process, the photosensitizer transitions from the ground state to a single reexcited state by absorbing photons of a specific wavelength, and then through intersystem translocation to a triple excited state. The excitons of the triple excited state then undergo energy transfer (type II photoreaction) or electron transfer (type I photoreaction) with the surrounding oxygen molecules or biomolecules. Biotoxic reactive oxygen species (ROS) are generated to achieve killing and treatment [6-7]. $^1O_2$ generated by type II light reaction can oxidize major biomolecules of nuclear membrane and cell membrane, such as unsaturated lipids and amino acids of proteins, and cause cell apoptosis, so $^1O_2$ is toxic [8].

Although PDT possesses the aforementioned advantages, achieving enhanced clinical efficacy remains a significant challenge. In this regard, precise selection and design of photosensitizers play a crucial role in determining the therapeutic outcomes of PDT [9]. The ability of traditional organic small molecules to transduce between systems has great limitations compared with excessive metal complexes. Iridium complexes, compared to other transition metal complexes, exhibit excellent photochemical and physical stability, large Stokes shift, and high intersystem crossover ability [10]. Consequently, they have emerged as extensively utilized transition metal complex materials across various domains such as bioimaging, electroluminescence, and photodynamic therapy [11-15].

Preprints (www.preprints.org) | NOT PEER-REVIEWED | Posted: 7 November 2023 doi:10.20944/preprints202311.0430.v1

Notably, iridium complexes have been extensively investigated as photosensitizers in photodynamic therapy [16, 17]. For instance, we successfully synthesized UCNPs@Ir-2-N—a near-infrared absorbing photosensitizer—by combining an AIE iridium complex with upconversion nanoparticles (UCNPs). This study demonstrates the promising application potential of metal iridium complex PSs in PDT [18].

Traditional small molecule photosensitizers, such as porphyrins[19], typically possess large planar conjugated structures and tend to aggregate in aqueous environments due to π-π interactions between molecules. This aggregation-induced quenching (ACQ) phenomenon significantly diminishes their photosensitization ability and severely limits their practical applications [20,21]. Furthermore, the fluorescence emitted by conventional photosensitizers is usually non-luminescent, leading to reduced imaging sensitivity [22, 23] and substantial constraints on the clinical application of many PSs in photodynamic therapy (PDT). In 2001, Academician Tang's research group discovered an opposing phenomenon to ACQ: under dilute solution conditions, these photosensitizers emit minimal light but exhibit enhanced emission upon concentration [24]. Unlike ACQ-based photosensitizers, those with aggregation-induced luminescence (AIE) properties generally possess non-planar structures. In the aggregated state, limited intramolecular motion reduces non-radiative energy dissipation while enhancing fluorescence emission and sensitizing a significant amount of reactive oxygen species (ROS), thereby offering substantial advantages for image-guided PDT [25-27]. However, there are few examples of iridium complexes with AIE properties used in photodynamic therapy. Therefore, the development of iridium-based AIE-active photosensitizers holds great significance for advancing PDT applications.

In this study, we developed and synthesized an iridium complex called **Ir-TPA** by incorporating a quinoline triphenylamine ligand. We conducted comprehensive investigations on the photophysical properties, AIE characteristics, spectral properties, and singlet oxygen generation capacity of **Ir-TPA**. As scheme 1, Our findings demonstrate that **Ir-TPA** exhibits excellent optical properties, displays remarkable AIE behavior, and possesses strong capability in generating reactive oxygen species. This research confirms the significant potential of AIE properties in enhancing the effectiveness of photodynamic therapy and presents a fresh perspective on utilizing iridium complexes in the field of photodynamic therapy.

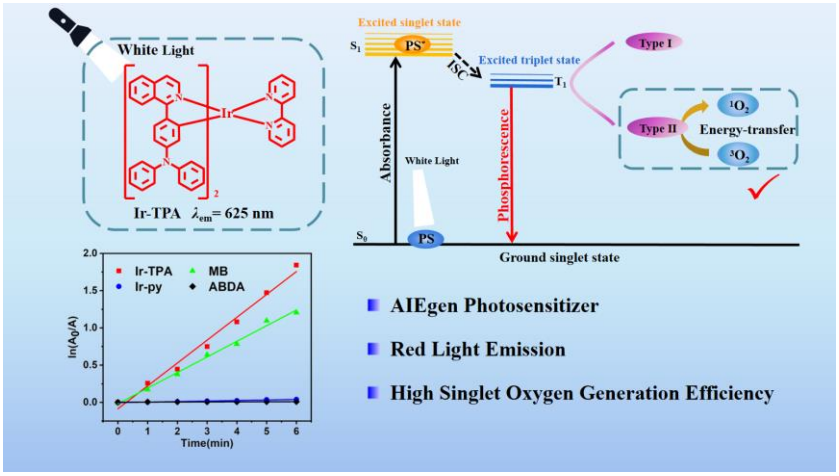

Scheme 1. Structure of **Ir-TPA** and schematic diagram of **Ir-TPA** producing singlet oxygen.

2. Results and Discussion

2.1. Analysis of photophysical properties of complexes

The photophysical properties of **Ir-TPA** and **Ir-py** were analyzed by ultraviolet absorption and fluorescence emission spectra. As shown in Figure 1, similar to the iridium complexes reported in the literature, **Ir-TPA** has two characteristic absorption peaks in a certain wavelength range. There is a strong characteristic absorption peak in the wavelength range of 250 ~ 350 nm, which is caused by the central charge (^{1}LC, π-π*) transition of the ligand in the metal iridium complex. There is a weak absorption band in the 350 nm to visible light band, which can be attributed to metal-ligand charge transfer transition (MLCT) and ligand-ligand charge transfer (LLCT) of the metal iridium complex

Preprints (www.preprints.org) | NOT PEER-REVIEWED | Posted: 7 November 2023 doi:10.20944/preprints202311.0430.v1

[28]. It can be clearly seen from the figure that the molar absorption coefficient of **Ir-TPA** was significantly enhanced compared with **Ir-py** after the introduction of the quinoline triphenylamine ligand (Table 1). Especially in the 425 nm visible region, the molar coefficient of **Ir-TPA** is 35900 $m^{-1}cm^{-1}$, which is eight times that of **Ir-py**. It can be shown that the absorption peak of iridium complex is obviously enhanced after the introduction of quinoline triphenylamine ligand. Subsequently, we determined the photoluminescent quantum yields (PLQYs) and excited state lifetimes of **Ir-TPA** and **Ir-py**, and summarized the corresponding photophysical data in Table 1. It can be seen from the data in the table that **Ir-TPA** and **Ir-py** have good photophysical properties.

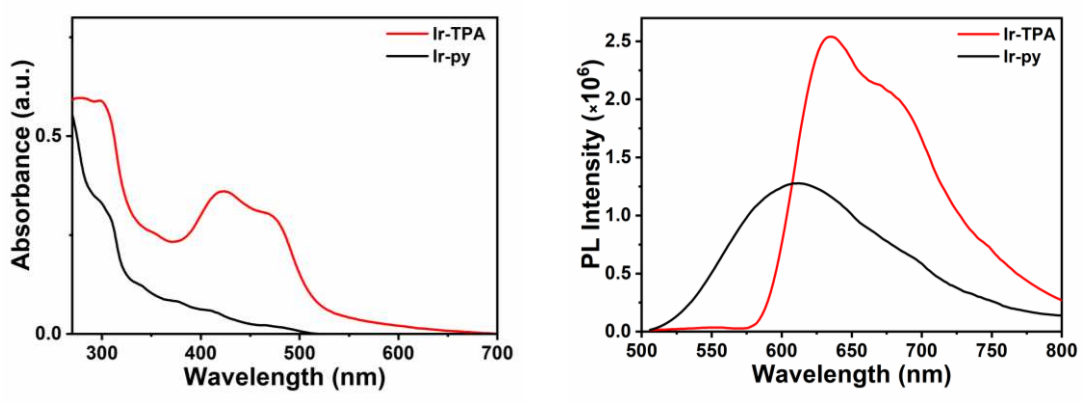

(**a**) (**b**)

Figure 1. a)Uv absorption spectra of **Ir-TPA**[1], **Ir-py**[2] (10^{-5} M) in CH_3CN/ H_2O (V/V=1/1); **b**) Fluorescence emission spectra, [1] λ_{ex}= 467 nm [2] λ_{ex}= 395 nm

Table 1. Photophysical data of **Ir-TPA** and **Ir-py**

	Λ_{abs} (nm)	λ_{em} (nm)	Φ_p (%)	T_p (ns)	K_r ($\times10^5$ S^{-1})	K_{nr} ($\times10^6$ S^{-1})	ε ($m^{-1}\cdot cm^{-1}$)
Ir-TPA [1]	300；425；470	625	7.22	169.7	4.25	5.4	59084；35900；30239
Ir-py [2]	310	590	2.07	57.9	3.5	16.9	28127

[1] determined at CH_3CN/ H_2O (v/v = 1/1) with a concentration of 1.0×10^{-5} M , λ_{ex} = 467 nm. [2] determined at CH_3CN/ H_2O (v/v = 1/1) with a concentration of 1.0×10^{-5} M , λ_{ex} = 395 nm.

2.2. Analysis of AIE properties of complexes

The AIE properties of **Ir-TPA** and **Ir-py** were analyzed in CH_3CN and water mixed system solution (water content ranged from 0 to 99%). As shown in Figure 2, **Ir-py** exhibited weak emission in pure CH_3CN solution, but with the increase of water content, the luminescence gradually weakened, showing obvious aggregation-induced quenching phenomenon. Iridium complexe **Ir-TPA** was obtained by using quinoline triphenylamine derivatives as cyclometalated ligands, which basically did not emit light in pure CH_3CN. The luminescence of **Ir-TPA** increased gradually with the increase of water content of bad solvent. When the water content of the mixed solution reaches 80%, **Ir-TPA** emits bright red light, and **Ir-TPA** has typical AIE characteristics.

Ir-TPA showed more emission redshift than **Ir-py** due to the better conjugation of cyclometal ligands derived from quinoline triphenylamine. **Ir-TPA** exhibit excellent red light emission and larger Stokes shifts value, indicating that in future biological experiments, autofluorescence interference will be effectively avoided, and the signal-to-noise ratio of imaging will be improved, which has a broad prospect in future biological applications.

Preprints (www.preprints.org) | NOT PEER-REVIEWED | Posted: 7 November 2023 doi:10.20944/preprints202311.0430.v1

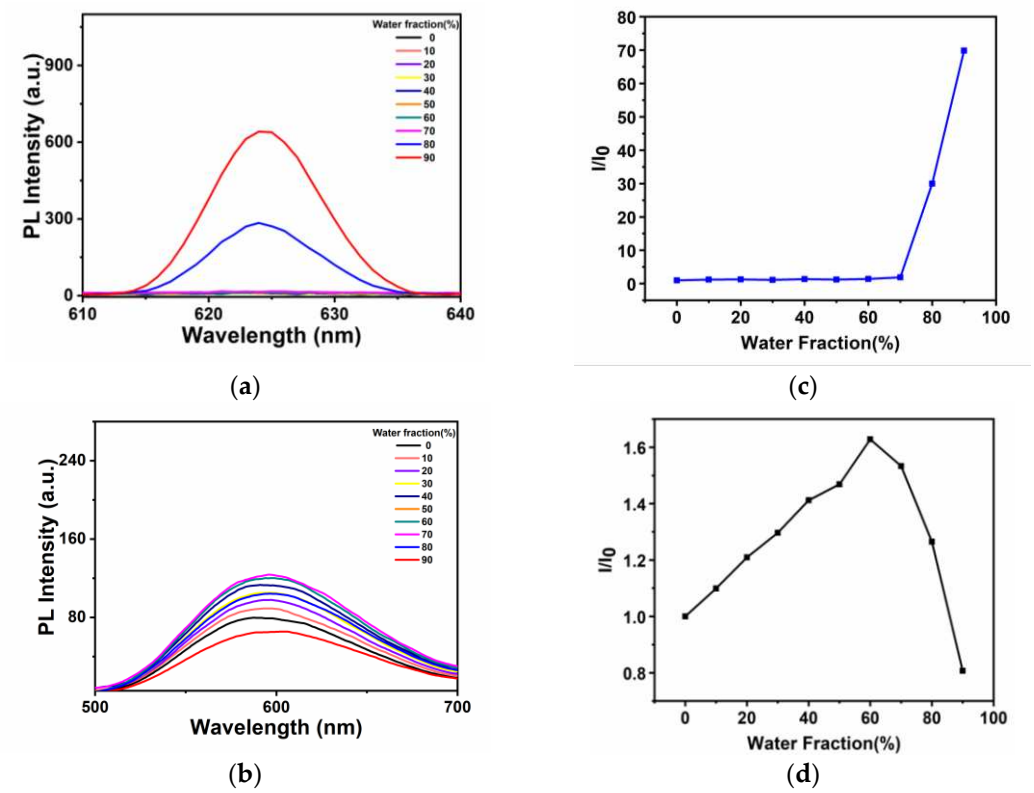

Figure 2. a) **Ir-TPA**[1], **b**) **Ir-py**[2] fluorescence emission spectra in different proportions of CH_3CN/ H_2O, I/I_0 value image of **c**） **Ir-TPA**、**d**） **Ir-py.** [1] λ_{ex}= 467 nm [2] λ_{ex}= 395 nm

Then we further investigated the AIE phenomena of **Ir-TPA** by UV-Vis absorption spectra. As can be seen from Figure 3, with the gradual increase of water content in the system, the tail of the absorption spectrum slightly warped, indicating that the Mi scattering phenomenon occurred [29]. Through the above experimental results, we can conclude that the complexe **Ir-TPA** have good AIE properties due to the emission enhancement caused by aggregation in poor solvents.

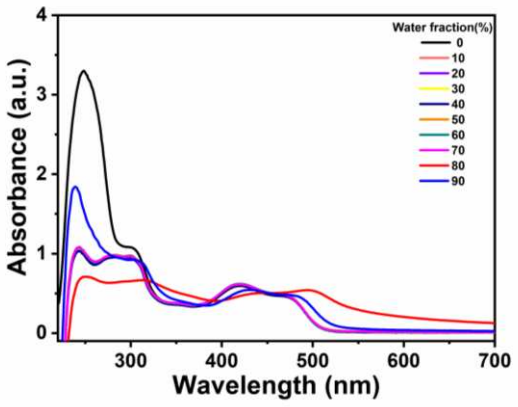

Figure 3. Ultraviolet-visible absorption spectra of **Ir-TPA** (10^{-5} M) in CH_3CN and H_2O mixed solutions.

2.3. Analysis of singlet oxygen generation capacity in solution

The ability of photosensitizer to produce singlet oxygen is very important for the effect of photodynamic therapy. The singlet oxygen production capacity of two iridium complexes **Ir-TPA** and **Ir-py** at CH_3CN:H_2O (V:V=1:9) was evaluated by monitoring the absorbance change of ABDA at 380 nm using ABDA as an indicator. As shown in Figure 4--6, for 1) the light group containing PSs; 2) Unilluminated group containing PSs and ABDA; 3) For the ABDA light group alone, the absorption intensity basically did not change during the time of illumination 360 s, which proves that **Ir-TPA** and **Ir-py** have good light stability. As shown in Figure 7, when irradiated with a white LED lamp,

Preprints (www.preprints.org) | NOT PEER-REVIEWED | Posted: 7 November 2023 doi:10.20944/preprints202311.0430.v1

the absorption of **Ir-TPA** and **Ir-py** at 380 nm is significantly reduced, which proves the production of singlet oxygen under the illumination condition. As shown in Figure 8, the singlet oxygen generation capacity of **Ir-TPA** and **Ir-py** both conform to the first-order kinetic equation. The higher the slope, the stronger the singlet oxygen generation capacity, and the singlet oxygen generation efficiency is **Ir-TPA**> Methylene Blue (MB)> **Ir-py**. As shown in Table 2, using methylene blue as the reference, the $^1O_2$ quantum yield of **Ir-TPA** is as high as 83.5%, indicating that **Ir-TPA** can efficiently produce singlet oxygen, and they will play an important role in the application of PDT cancer as Ps.

Table 2. Singlet oxygen generation efficiency data of **Ir-TPA, Ir-py** and MB.

	Linear fit slope	Intercept	Singlet oxygen yield(%)
Ir-TPA	0.30687	0.08544	83.5
Ir-py	0.00701	0.00288	24.0
MB	0.20943	0.01792	52.0

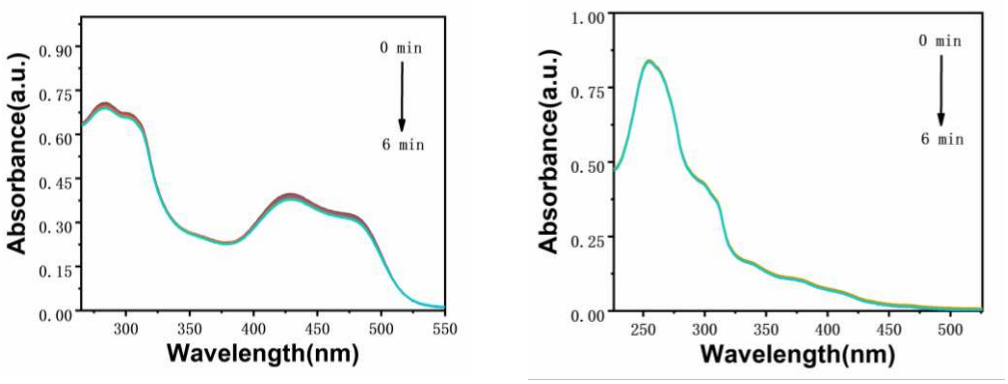

(**a**) (**b**)

Figure 4. Ultraviolet absorption spectra of a) **Ir-TPA**; b)**Ir-py** (25 μM) under white light (400-700 nm, 20 mW cm^{-2})

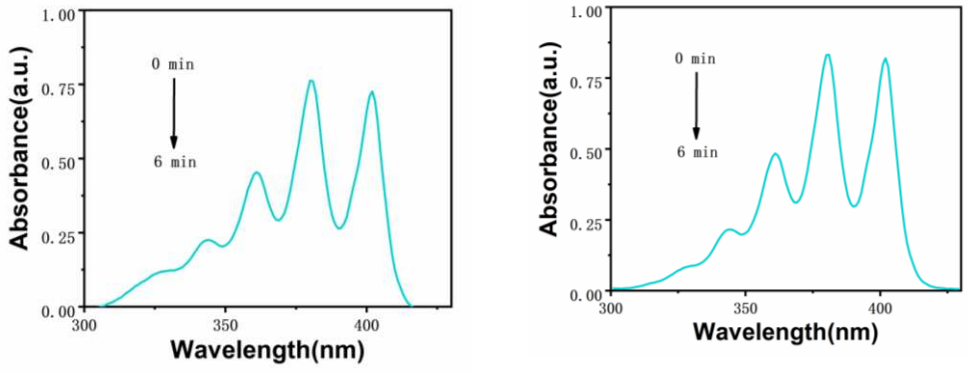

(**a**) (**b**)

Figure 5. Ultraviolet-visible absorption spectra of ABDA (30 μg.mL^{-1}) without light in the presence of a) **Ir-TPA**; b) **Ir-py** (25 μM)

Preprints (www.preprints.org) | NOT PEER-REVIEWED | Posted: 7 November 2023 doi:10.20944/preprints202311.0430.v1

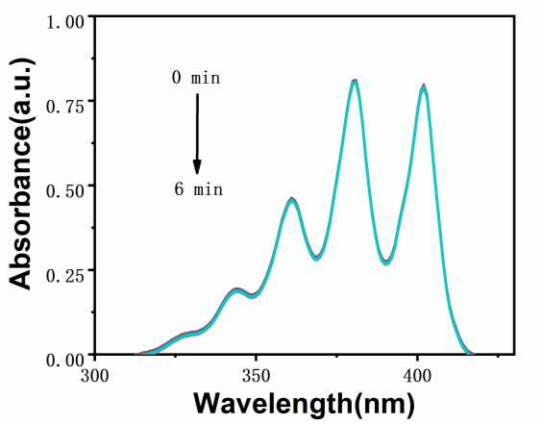

Figure 6. Ultraviolet-visible absorption spectra of ABDA under white light (400-700 nm, 20 mW cm^{-2})

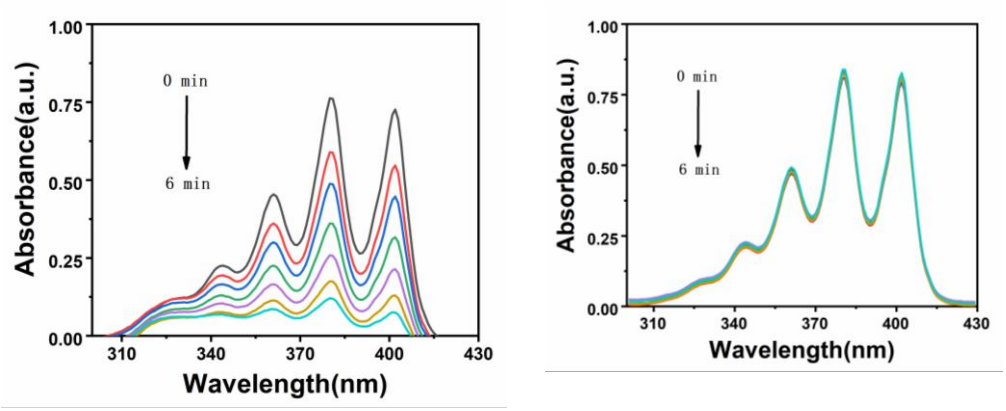

(**a**) (**b**)

Figure 7. Ultraviolet-visible absorption spectra of ABDA(30 μg.mL^{-1}) under the irradiation of a white light LED lamp (400-700 nm, 20 mW cm^{-2}) in the presence of a) **Ir-TPA**; b) **Ir-py** (25 μM)

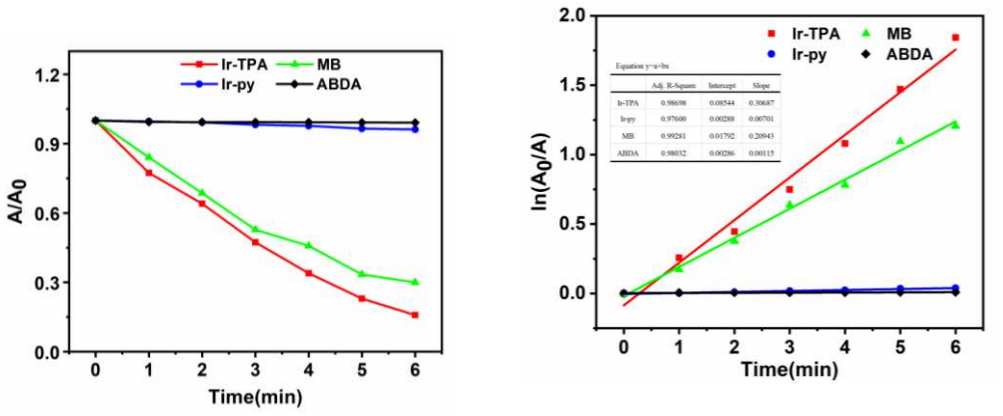

(**a**) (**b**)

Figure 8. In the presence of **Ir-TPA**/ **Ir-py**/ MB (25μM), under the condition of illumination (400-700 nm, 20 mW cm^{-2}), a) the radiation attenuation curve of ABDA at 380 nm at different times; b) Time-dependent generation kinetics curve of $^1O_2$

3. Materials and Methods

3.1. General Information

Reagents and solvents should be used as received from the supplier. Unless otherwise specified, all purification is performed using 200-300 mesh silica gel from the supplier by column

Preprints (www.preprints.org) | NOT PEER-REVIEWED | Posted: 7 November 2023 doi:10.20944/preprints202311.0430.v1

chromatography. The structure was confirmed by Bruker AV600 NMR spectrometer and Bruker autoFlex III mass spectrometer. A Shimadzu UV-3100 spectrophotometer was used for ultraviolet-visible experiments. The fluorescence emission spectra were measured by Edinburgh FLS920 steady-state transient fluorescence spectrometer.

3.2. Spectral test method

The spare solution of **Ir-TPA** and **Ir-py** (1 mM) was prepared in acetonitrile. The preparation method of the test solution is as follows: During the test, 30 μL **Ir-TPA** and **Ir-py** reserve solution, 270 μL acetonitrile and 2700 μL ultra-pure water are prepared into the test solution with a total volume of 3 mL.

3.3. Test method for singlet oxygen in solution

The efficacy of photodynamic therapy is evaluated by the level of singlet oxygen production in the solution. The $^1O_2$ formation capacity of **Ir-TPA**/ **Ir-py** at CH_3CN/ H_2O=1/9 was evaluated using 9, 10-anthracenedi-bis (methylene) dicarboxylic acid (ABDA) as an indicator. After a certain time of light irradiation, the absorbance of ABDA at 380 nm was significantly reduced, indicating that the photosensitizer sensitized oxygen to produce $^1O_2$. In this experiment, CH_3CN/ H_2O=1/9 solution containing **Ir-TPA**/ **Ir-py** (25 μM) was prepared and mixed with ABDA (30 μg.mL^{-1}), and then exposed to white light (400-700 nm, 20 mW cm^{-2}) for irradiation. The absorption intensity of ABDA at 380 nm was monitored every 60 s.

3.4. Synthesis and characterization of complexes

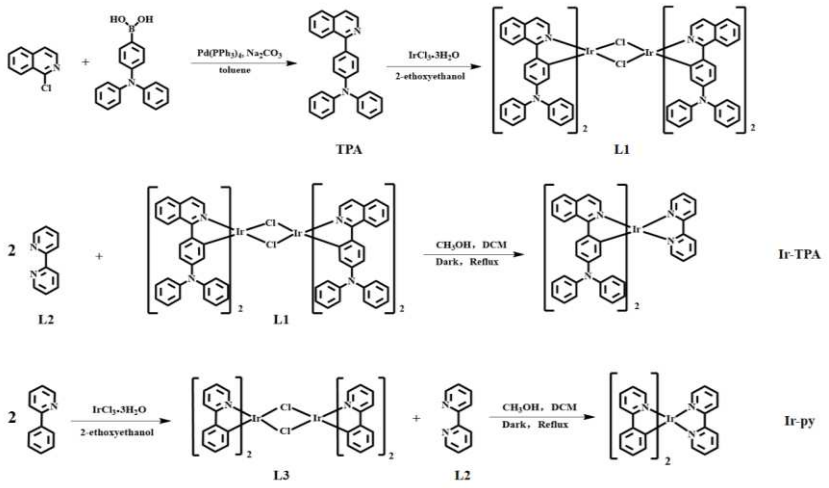

Figure 9. Iridium(III) complex synthesis route.

3.3.1. Synthesis of cyclometalated ligand TPA

Trianiline 4-borate (0.972 g, 3.36 mmol) and 1-chloroisoquinoline (0.496 g, 3.06 mmol) were dissolved in 30 mL toluene, and the catalyst tetrtriphenylphosphine palladium (0.177 g, 0.15 mmol) and 2 mol/L sodium carbonate solution 20 mL were added. The reaction was kept at 110℃ for 48 h in deoxygenated environment. After the reaction, the organic phase was extracted and dried with anhydrous magnesium sulfate, filtered and purified by silica gel column chromatography (dichloromethane/petroleum ether, 10/5). The product is a light yellow solid with a yield of 68%. ^{1}H NMR (500 MHz, $CDCl_3$) δ 8.59 (d, J = 5.7 Hz, 1H), 8.23 (d, J = 8.5 Hz, 1H), 7.87 (d, J = 8.2 Hz, 1H), 7.69 (t, J = 7.2 Hz, 1H), 7.62 – 7.59 (m, 3H), 7.56 (t, J = 7.7 Hz, 1H), 7.29 (t, J = 7.9 Hz, 4H), 7.21 (dd, J = 13.3, 8.1 Hz, 6H), 7.05 (d, J = 7.3 Hz, 2H).

3.3.2. Synthesis of L1

TPA (0.930 g, 2.5 mmol) and $IrCl_3$·$3H_2O$ (0.317 g, 1 mmol) were dissolved in a mixed solution of 30 mL ethylene glycol ether and 10 mL water, and the reaction was continued for 24 h at 120℃ under

 doi:10.20944/preprints202311.0430.v1

nitrogen atmosphere. At the end of the reaction, water was added to the round-bottom flask and continued to stir for 30 min. The Brinell funnel was used for pumping and filtering, and the obtained solids were put into the oven for 24 h. After drying, the product became a deep red solid with a yield of 80%. The product is directly used in subsequent reactions.

3.3.5. Synthesis of Ir-TPA

L1 (0.194 g, 0.1 mmol) and **L2** (0.0312 g, 0.2 mmol), methanol 20 mL and dichloromethane 20 mL were added as mixed solvents in single-mouth bottles, respectively. N_2 was charged for protection under dark conditions, and reflux was carried out at 78℃for 8 h. At the end of the reaction, solid potassium hexafluorophosphate (1 mmol, 0.184 g) was added to the bottle, stirring for 45 minutes, and then the solvent was filtered and spun dry. The solid is dissolved in a small amount of dichloromethane, and the precipitation is obtained by filtration after reverse precipitation with petroleum ether. The crude product was purified by silica gel column chromatography (methylene chloride/acetone, 10/8). The product is a dark red solid with a yield of 35%. ^{1}H NMR (600 MHz, $CDCl_3$) δ 8.74 – 8.72 (m, 1H), 8.66 (d, J = 8.2 Hz, 1H), 8.14 (t, J = 7.8 Hz, 1H), 8.02 (d, J = 8.9 Hz, 1H), 7.88 (d, J = 5.2 Hz, 1H), 7.66 (t, J = 4.9 Hz, 3H), 7.46 – 7.44 (m, 1H), 6.98 (dd, J = 13.5, 6.8 Hz, 6H), 6.92 (d, J = 7.9 Hz, 4H), 6.81 (t, J = 6.6 Hz, 3H), 6.76 (dd, J = 8.8, 2.3 Hz, 1H). ESI-MS: [m/z] = 1091.3508 (calcd: 1091.35).

3.3.6. Synthesis of Ir-py

Dissolve **L3** (0.1608 g, 0.1 mmol) and **L2** (0.0312 g, 0.2 mmol), methanol 20 mL and dichloromethane 20 mL as mixed solvents in a single mouth bottle. N_2 was charged for protection under dark conditions, and reflux was carried out at 78℃ for 8 h. At the end of the reaction, solid potassium hexafluorophosphate (1 mmol, 0.184 g) was added to the bottle, stirring for 45 minutes, and then the solvent was filtered and spun dry. The solid is dissolved in a small amount of dichloromethane, and the precipitation is obtained by filtration after reverse precipitation with petroleum ether. The yellow solid was obtained after drying, and the yield was 44%.^{1}H NMR (600 MHz, DMSO) δ 8.89 (d, J = 8.2 Hz, 1H), 8.28 (t, J = 7.2 Hz, 2H), 7.95 – 7.91 (m, 2H), 7.88 (d, J = 5.3 Hz, 1H), 7.72 – 7.69 (m, 1H), 7.62 (d, J = 5.7 Hz, 1H), 7.16 (t, J = 6.6 Hz, 1H), 7.03 (t, J = 7.5 Hz, 1H), 6.91 (t, J = 7.4 Hz, 1H), 6.20 (d, J = 7.6 Hz, 1H). ESI-MS: [m/z] = 657.1636 (calcd: 657.16).

4. Conclusions

The iridium metal complex **Ir-TPA**, possessing aggregation-induced emission (AIE) properties, was designed and synthesized in this study. By incorporating quinoline triphenylamine metallized ligands, the AIE properties of **Ir-TPA** were enhanced, leading to a significant improvement in the complex's absorption capacity. Notably, the complex exhibited red light emission with a maximum wavelength of 625 nm. In-depth investigations were conducted on the photophysical properties, AIE characteristics, spectral features, and reactive oxygen generation capability of **Ir-TPA**. The results demonstrated that **Ir-TPA** displayed excellent optical properties along with pronounced AIE behavior and strong reactive oxygen species production ability. This work validates the substantial potential of AIE properties in enhancing photodynamic therapy efficacy and provides novel insights into the application of iridium complexes in this field.

Supplementary Materials: The following supporting information can be downloaded at: www.mdpi.com/xxx/s1.

Author Contributions: Conceptualization, W.Z. and D.Z.; methodology, W.Z.; software, W.Z. and Z.W.; validation, W.Z., S.L. and Q.Z.; formal analysis, W.Z.; investigation, W.Z. and Z.W.; resources, W.Z.; data curation, W.Z.; writing—original draft preparation, W.Z.; writing—review and editing, W.Z. and D.Z.; project administration, W.Z.; funding acquisition, D.Z. All authors have read and agreed to the published version of the manuscript.

Funding: This research was funded by NSFC (Grant No. 52073045), the Development and Reform Commission of Jilin Province (2020C035-5), and Changchun Science and Technology Bureau (21ZGY19).

Data Availability Statement: All data generated or analyzed during this study are included in this published article and its supplementary information files.

Conflicts of Interest: The authors declare no conflict of interest.

References

1. Cheng H B, et al. Protein-Activatable Diarylethene Monomer as a Smart Trigger of Noninvasive Control Over Reversible Generation of Singlet Oxygen: A Facile, Switchable, Theranostic Strategy for Photodynamic-Immunotherapy [J]. *J Am Chem Soc*, **2021**, 143(5): 2413-2422.
2. Kwiatkowski S, et al. Photodynamic therapy - mechanisms, photosensitizers and combinations [J]. *Biomed Pharmacother*, **2018**, 10, 1098-1107.
3. Liu S, et al. Recent advances of AIE light-up probes for photodynamic therapy [J]. *Chemical Science*, **2021**, 12(19): 6488-6506.
4. Kang M, et al. Evaluation of structure-function relationships of aggregation-induced emission luminogens for simultaneous dual applications of specific discrimination and efficient photodynamic killing of gram-positive bacteria [J]. *Journal of the American Chemical Society*, **2019**, 141(42): 16781-16789.
5. Wang C,et al. A receptor-targeting AIE photosensitizer for selective bacterial killing and real-time monitoring of photodynamic therapy outcome [J]. *Chemical Communications*, **2022**, 58(50): 7058-7061.
6. Zhao X, et al. Recent progress in photosensitizers for overcoming the challenges of photodynamic therapy: from molecular design to application [J]. *Chemical Society Reviews*, **2021**, 50(6): 4185-4219.
7. Pham T C, et al. Recent strategies to develop innovative photosensitizers for enhanced photodynamic therapy [J]. *Chemical Reviews*, **2021**, 121(21): 13454-13619.
8. Li X, et al. Phthalocyanines as Medicinal Photosensitizers: Developments in the Last Five Years [J]. *Coordin Chem Rev*, **2019**, 379: 147-160.
9. Kenry, et al. Enhancing the Theranostic Performance of Organic Photosensitizers with Aggregation-Induced Emission [J]. *Accounts of Materials Research*, **2022**, 3(7): 721-734.
10. Ma D, et al. Recent Progress in Sublimable Cationic Iridium(III) Complexes for Organic Light-Emitting Diodes [J]. *Chem Rec*, **2019**, 19(8): 1483-1498.
11. Yang P, et al. Synthesis of pH-responsive cyclometalated iridium(III) complex and its application in the selective killing of cancerous cells [J]. *Dalton Trans*, **2021**, 50(46): 17338-17345.
12. Zhou L,et al. Enhancing the ROS generation ability of a rhodamine-decorated iridium(iii) complex by ligand regulation for endoplasmic reticulum-targeted photodynamic therapy [J]. *Chem Sci*, **2020**, 11(44): 12212-12220.
13. Han Z, et al. A Novel Luminescent Ir(III) Complex for Dual Mode Imaging: Synergistic Response to Hypoxia and Acidity of Tumor Microenvironment [J]. *Chem Commun*, **2020**, 56(58), 8055-8058.
14. Gao F, et al. Photoactivated Nanosheets Accelerate Nucleus Access of Cisplatin for Drug-Resistant Cancer Therapy [J]. *Adv Funct Mater*, **2020**, 30(49): 2001546.
15. Rashid, A., et al. Development and Application of Ruthenium(II) and Iridium(III) Based Complexes for Anion Sensing [J]. *Molecules*, **2023**, 28(3).
16. Jiang J, et al. Enhancing Singlet Oxygen Generation in Semiconducting Polymer Nanoparticles Through Fluorescence Resonance Energy Transfer for Tumor Treatment [J]. *Chem Sci*, **2019**, 10(19): 5085-5094.
17. Cabrera-González J, et al. Multinuclear Ru(ii) and Ir(iii) Decorated Tetraphenylporphyrins as Efficient PDT Agents [J]. *Biomater Sci*, **2019**, 7(8): 3287-3296.
18. Liu S, et al. AIE-active iridium(III) complex integrated with upconversion nanoparticles for NIR-irradiated photodynamic therapy [J]. *Chem Commun (Camb)*, **2022**, 58(72): 10056-10059.
19. Tsolekile, et al. Porphyrin as Diagnostic and Therapeutic Agent [J]. *Molecules*, **2019**, 24, 2669.
20. Jia S, et al.Design and structural regulation of AIE photosensitizers for imaging-guided photodynamic anti-tumor application [J]. *Biomaterials Science*, **2022**, 10(16): 4443-4457.
21. Yan D, et al. Innovative Synthetic Procedures for Luminogens Showing Aggregation-Induced Emission [J]. *Angew.Chem.Int. Ed.*, **2021**, 60, 15724–15742
22. Luby B M, et al. Advanced Photosensitizer Activation Strategies for Smarter Photodynamic Therapy Beacons [J]. *Angew Chem Int Ed Engl*, **2019**, 58(9): 2558-2569.
23. Wu W, et al. Controllable Photodynamic Therapy Implemented by Regulating Singlet Oxygen Efficiency [J]. *Adv Sci (Weinh)*, **2017**, 4(7): 1700113-1700134.
24. Luo J, et al. Aggregation-induced emission of 1-methyl-1,2,3,4,5-pentaphenylsilole [J]. *Chem. Commun.*, **2001**, 1740-1741.
25. Zha M, et al. Recent advances in AIEgen-based photodynamic therapy and immunotherapy [J]. *Advanced Healthcare Materials*, **2021**, 10 (24): 2101066.
26. Mei J, et al. Aggregation-induced emission: together we shine, united we soar! [J]. *Chemical Reviews*, **2015**, 115(21): 11718-11940.
27. Xue K, et al. A sensitive and reliable organic fluorescent nanothermometer for noninvasive temperature sensing [J]. *Journal of the American Chemical Society*, **2021**, 143(35): 14147-14157.
28. Ulbricht, C., et al. Recent Developments in the Application of Phosphorescent Iridium(III) Complex Systems [J]. *Advanced Materials*, **2009**, 21(44): 4418-4441.

 doi:10.20944/preprints202311.0430.v1

29. Xu, B., et al. Achieving very bright mechanoluminescence from purely organic luminophores with aggregation-induced emission by crystal design [J]. *Chem Sci*, **2016**, 7(8): 5307-5312.